

Quantum non-Markovian behavior at the chaos border

Ignacio García-Mata,^{1,2} Carlos Pineda,³ and Diego Wisniacki⁴

¹*Instituto de Investigaciones Físicas de Mar del Plata (IFIMAR, CONICET),
Universidad Nacional de Mar del Plata, Mar del Plata, Argentina.**

²*Consejo Nacional de Investigaciones Científicas y Tecnológicas (CONICET), Argentina*

³*Instituto de Física, Universidad Nacional Autónoma de México, México D.F., 01000, México*

⁴*Departamento de Física “J. J. Giambiagi”, FCEN, Universidad de Buenos Aires, 1428 Buenos Aires, Argentina*

(Dated: submitted on May 27, 2013)

In this work we study the non-Markovian behavior of a qubit coupled to an environment in which the corresponding classical dynamics change from integrable to chaotic. We show that in the transition region, where the dynamics has both regular islands and chaotic regions, the average non-Markovian behavior is enhanced to values even larger than in the regular region. This effect can be related to the non-Markovian behavior as a function of the the initial state of the environment, where maxima are attained at the regions dividing separate areas in classical phase space, particularly at the borders between chaotic and regular regions. Moreover, we show how the measure of non-Markovian behavior gives a precise image of the classical phase portrait.

PACS numbers: 03.65.Yz,05.45.Mt,05.45Pq

I. INTRODUCTION

The unavoidable effect of uncontrollable degrees of freedom on a quantum system are of primal interest for both fundamental and practical reasons. On one hand, they provide a framework in which the transition from a quantum to a classical description of nature can be studied, and on the other, they are the most important limiting factor in the realization of the technologies promised by the field of quantum information. This effect is known as decoherence [1], and is commonly associated with a monotonic loss of coherence in the off-diagonal terms in the density matrix. However monotonic loss of coherence is only one side of the story which results from approximations such as weak coupling and a vanishing correlation time in the environment. This is the so called Markov approximation, usually related to information flowing only from the system to the environment and not backward. The Markov approximation leads to the Lindblad master equation and quantum dynamical semigroups [2, 3], also known as quantum Markovian dynamics. Lately, though, interest in problems where the Markov approximation is no longer valid has flourished (see [4–11], to name just a few). One very interesting feature of non-Markovian evolution is that information backflow can bring back coherence to the physical system and sometimes even preserve it [12, 13]. The simulation of non-Markovian dynamics and the transition from Markovian to non-Markovian has been recently reported in experiments [14–16].

Although there has been much activity in this context in the last years, basic question remain untouched. In this context there is the critical question of the influence of the underlying classical dynamics of the environment on the central system. Intuition indicates that a

chaotic environment should result in Markovian dynamics and a regular (or integrable) environment in strong non-Markovian effects. In [17] this transition has been studied. Understanding the case where the environment has associated classical dynamics consisting of a mixture of regular islands, broken tori and hyperbolic dynamics, remains an open problem. The importance of this case is not to be overlooked being that mixed systems are the rule rather than the exception [18]. The purpose of this work is then to shed some light on the relation between the classical dynamics of the environment, for environments where the transition from regular to chaotic is tuneable by a parameter. The complexities of such systems make analytical treatment almost impossible so we shall mainly focus on numerical simulations.

We center on a system consisting on a qubit coupled with an environment in a pure dephasing fashion. In such a way that the environment evolution is conditioned by the state of the qubit [8, 9, 17, 19–22]. The qubit acts as a probe that can be used to extract important information from the dynamics of the environment [23]. As environment we use paradigmatic examples of quantum chaos: quantum maps on the torus. In particular we focus kicked maps which by changing one parameter one can go from integrable to chaotic.

One of the keys of studying non-Markovian behavior is to have an efficient way to quantify it or measure it. For this kind of setup, we find that the best adapted was defined in [6]. It can be directly linked to the fidelity decay of the environment [9, 17]. Fidelity and its decay is a vastly studied quantity especially because it can be used to characterize quantum chaotic systems [24–26] but also because it is a readily measurable quantity [27]. Using this measure we found that the transition from integrable (“non-Markovian”) to chaotic (“Markovian”) is not smooth. Typically, in the transition there is a maximum which can be larger than the value that this measure attains for the regular dynamics. But more im-

* i.garcia-mata@conicet.gov.ar

portantly, that the maximum happens at a value of the parameter that is critical in the corresponding classical dynamics, like the breakup of the last irrational torus, and the onset of unbound diffusion. The maxima are obtained by averaging over a complete set of states and therefore characterize global non-Markovian behavior as a function of one parameter.

We also studied local non markovian behavior by taking the environment initially in a pure Gaussian (“localized”) state. In our model, non-Markovian behavior is essentially given by the fluctuations in the the fidelity of the environment. We observe that the non-Markovian measure (given by these fidelity fluctuations) reproduce the intricate structure of the classical phase space with extraordinary precision. Moreover, we observe that the non-Markovian measure as a function of position in phase space has maxima in the regions where that are neither chaotic nor regular, i.e. at the borders between chaos and regularity. This establishes the non-Markovianity measure used, which depends on the long time fidelity fluctuations, as pointer to the chaos border. Another way of identifying this border can be found in [28]. As a consequence, our results contribute to a deeper understanding of the fidelity decay of quantum systems with mixed classical dynamics, which is an open problem of current interest [26].

II. MEASURING NON-MARKOVIANITY USING FIDELITY

The discussion about non-Markovian behavior makes sense only if there is an efficient way to characterize it. There are many proposed measures. The most widely spread was proposed in [6] by Breuer, Laine and Piilo (BLP) and it is based on the distinguishability of quantum states. Rivas, Huelga and Plenio (RHP) [7] proposed two measures which are based on the evolution of entanglement to an ancilla, under trace preserving completely positive maps. There are others based on Fisher information [29] or the validity of the semigroup property [30]. For some situations [31] BLP and RHP are equivalent. [32] So here we only consider BLP.

To define the BLP measure we use the trace distance

$$D(\rho_1, \rho_2) = \frac{1}{2} \text{Tr} |\rho_1 - \rho_2| \quad (1)$$

which is a metric on the space of density matrices and can be interpreted as a measure of distinguishability [6]. The positive rate of change of this distance measure can be interpreted as the flow of information from the system to the environment. So non-Markovian behavior is quantified by

$$\mathcal{M} = \max_{\rho_{1,2}(0)} \int_{\sigma > 0} dt \sigma(t, \rho_{1,2}(0)), \quad (2)$$

where $\sigma(t, \rho_{1,2}(0)) = dD(\rho_1(t), \rho_2(t))/dt$.

A. Pure dephasing on one qubit: fidelity and non-Markovianity

We assume that that the interaction between the environment and the probe qubit is factorizable, and that it commutes with the internal hamiltonian of the qubit. Properly rearranged, one can write the hamiltonian of the form

$$H = |0\rangle\langle 0| \otimes H_0 + |1\rangle\langle 1| \otimes H_1, \quad (3)$$

were H_0 and H_1 act only on the environment and $|0\rangle\langle 0|$, $|1\rangle\langle 1|$ are projectors onto some orthonormal basis of the qubit [19]. This kind of pure dephasing interactions occur spontaneously in several experiments (for example [33]), but can also be engineered [34].

We suppose that initially system and environment are not correlated, which can be expressed as $\rho_{\text{sys,env}}(0) = \rho_{\text{sys}}(0) \otimes \rho_{\text{env}}$. To focus only on the system, the environment degrees of freedom should be traced out

$$\rho_{\text{sys}}(t) = \text{Tr}_{\text{env}} [U(t)\rho_{\text{sys}}(0) \otimes \rho_{\text{env}}U^\dagger(t)] \quad (4)$$

with

$$U(t) = |0\rangle\langle 0|U_0(t) + |1\rangle\langle 1|U_1(t). \quad (5)$$

This yields a dynamical map for the qubit that we write as

$$\rho_{\text{sys}}(t) = \Lambda(t)(\rho_{\text{sys}}(0)) \quad (6)$$

which, in the basis of Pauli matrices, takes the form

$$\Lambda = \begin{pmatrix} 1 & 0 & 0 & 0 \\ 0 & \text{Re}[f(t)] & \text{Im}[f(t)] & 0 \\ 0 & \text{Im}[f(t)] & \text{Re}[f(t)] & 0 \\ 0 & 0 & 0 & 1 \end{pmatrix}. \quad (7)$$

Here we have taken conventionally $\{\sigma_i\} = \{\mathbb{I}, \sigma_x, \sigma_y, \sigma_z\}$ and $\Lambda_{j,k} = (1/2)\text{Tr} [\sigma_j U(t)\sigma_k \otimes \rho_{\text{env}}U^\dagger(t)]$. In Eq. (7) $f(t) = \text{Tr}[\rho_{\text{env}}U_1(t)^\dagger U_0(t)]$ is the expectation value of the echo operator $U_1(t)^\dagger U_0(t)$. In this work we will assume that H_1 (U_1) is just a perturbation of H_0 (U_0). If ρ_{env} is pure then $|f(t)|^2$ is the well known quantity called Loschmidt echo [35] – also called fidelity – which can be used to characterize quantum chaos [24–26]

In our case, where the system is one qubit, the states that maximize \mathcal{M} are pure orthogonal states lying at the equatorial plane on the Bloch sphere. [36]. Here we consider two cases. If the state of the environment is a pure state [9] $\rho_{\text{env}} = |\psi\rangle\langle\psi|$ then we get

$$\begin{aligned} \mathcal{M}_p(t) &= 2 \int_{t=0, |f|>0}^t d\tau \frac{d|f(\tau)|}{d\tau} \\ &\equiv 2 \sum_i [|f(t_i^{(\max)})| - |f(t_i^{(\min)})|]. \end{aligned} \quad (8)$$

where $|f(t)| = |\langle\psi|U_1^\dagger(t)U_0(t)|\psi\rangle|$ is the square root of the Loschmidt echo and $t_i^{(\max)} > t_i^{(\min)}$ correspond to the

times of successive local maxima and minima of $|f(t)|$. \mathcal{M}_p is the quantity considered in [9].

On the other hand, if we have no knowledge or control over the environment, then it will most likely be in a mixed state. If we assume it is in a maximally mixed state (proportional to the identity) we get [17]

$$\mathcal{M}_m(t) = 2 \sum_i |\langle f(t_i^{(\max)}) \rangle - \langle f(t_i^{(\min)}) \rangle|, \quad (9)$$

where $\langle f(t) \rangle$ is the average fidelity amplitude. If the average is done over a complete set of states then

$$\langle f(t) \rangle = \frac{1}{N} \text{tr}[U_1^\dagger(t)U_0(t)] \quad (10)$$

which depends only on the set of states being complete, but not on the kind of states.

In the results that we present we model the dynamics of the environment $U_{0,1}$ using quantum maps on the torus with a finite Hilbert space. In this case, after some time the fidelity fluctuates around some constant value. This causes a linear growth with time of \mathcal{M}_p and \mathcal{M}_m (the slope goes to zero with the size of the Hilbert space). For this reason we follow the strategy of [17] and consider \mathcal{M}_m and \mathcal{M}_p up to some finite time t .

III. KICKED MAPS

For the numerical simulations we suppose that the dynamics of the environment is given by a quantum map on the torus. Apart from the fact that these maps are the simplest paradigmatic examples of quantum chaotic dynamics, the ones we consider can be very efficiently implemented using fast Fourier transform. Due to periodic boundary conditions the Hilbert space is discrete and of dimension N . This defines an effective Planck constant $\hbar = 1/(2\pi N)$. Position states can be represented as vertical strips of width $1/N$ at positions $q_i = i/N$ (with $i = 0, \dots, N-1$) and momentum states are obtained by discrete Fourier transform. A quantum map is simply a unitary U acting on an N dimensional Hilbert space. Quantum maps can be interpreted as quantum algorithms and vice-versa. In fact there exist efficient – i.e. better than classical – quantum algorithms for many of the well known quantum maps [37–42], making them interesting testbeds of quantum chaos in experiments using quantum simulators (e.g. [22, 40, 43]).

Here we consider two well known maps with the characteristic properties of kicked systems, i.e. they can be expressed as

$$U = T(\hat{p})V(\hat{q}). \quad (11)$$

They also share the property that by changing one parameter (the kicking strength) they can be tuned to go from classical integrable to chaotic dynamics.

The quantum (Chirikov) standard map (SM) [44]

$$U_K^{(\text{SM})} = e^{-i\frac{\hat{p}^2}{2\hbar}} e^{-i\frac{K}{\hbar} \cos(2\pi\hat{x})} \quad (12)$$

corresponds to the classical map

$$\begin{aligned} p_{n+1} &= p_n + \frac{K}{2\pi} \sin(2\pi x_n) \\ x_{n+1} &= x_n + p_{n+1}. \end{aligned} \quad (13)$$

Since we consider a toroidal phase space both equations are to be taken modulo 1. For small K dynamics is regular. Below a certain critical value K_c the motion in momentum is limited by invariant KAM curves. At $K_c = 0.971635\dots$ [45], the last KAM curve, with most irrational winding number, breaks. Above K_c there is unbounded diffusion in p . For very large K , there exist islands but the motion is essentially chaotic.

The quantum kicked Harper map (HM)

$$U_{K_1, K_2}^{(\text{HM})} = e^{-i\frac{K_1}{\hbar} \cos(2\pi\hat{p})} e^{-i\frac{K_2}{\hbar} \cos(2\pi\hat{x})} \quad (14)$$

is an approximation of the motion of kicked charge under the action of an external magnetic field [46, 47]. Equation (14) corresponds to the classical map

$$\begin{aligned} p_{n+1} &= p_n - K_1 \sin(2\pi x_n) \\ x_{n+1} &= x_n + K_2 \sin(2\pi p_{n+1}) \end{aligned} \quad (15)$$

For $k < 0.11$, the dynamics described by the associated classical map is regular, while for $k > 0.63$ there are no remaining visible regular islands [48].

In Fig. 1 we show examples of phase space portraits for the two maps for three different values of K where the transition from regular to mainly chaotic can be observed.

For the numerical calculations we take for the standard map $U_0 \equiv U_K^{(\text{SM})}$ and $U_1 \equiv U_{K+\delta K}^{(\text{SM})}$ and for the Harper map $U_0 \equiv U_{K,K}^{(\text{HM})}$ (notice $K_1 = K_2 = K$) and $U_1 \equiv U_{K,K+\delta K}^{(\text{HM})}$. So δK is the perturbation strength.

IV. NON-MARKOVIANITY AT THE FRONTIER BETWEEN CHAOS AND INTEGRABILITY

Both the SM and the HM offer the opportunity to explore the transition from integrability to chaos by changing the kicking parameter. By doing that (for the HM) two things were found in [17]. As expected, For very large K , which corresponds to chaotic dynamics, Markovian behavior was observed. On the other hand, for small K corresponding to regular dynamics, non-Markovian behavior was obtained. However, there was an unexpected result: the transition is not smooth. There is a clear peak in $\mathcal{M}_m(t)$ – Fig. 3 in [17] – that, depending on the value of δK and t can even be larger than the value for regular dynamics. To complement this previous result and further illustrate this effect we calculated $\mathcal{M}_m(t)$ as a function of K and δK . In particular, for very short times, the decay of the fidelity amplitude has a rich structure [49]. It can be shown by semiclassical calculations that

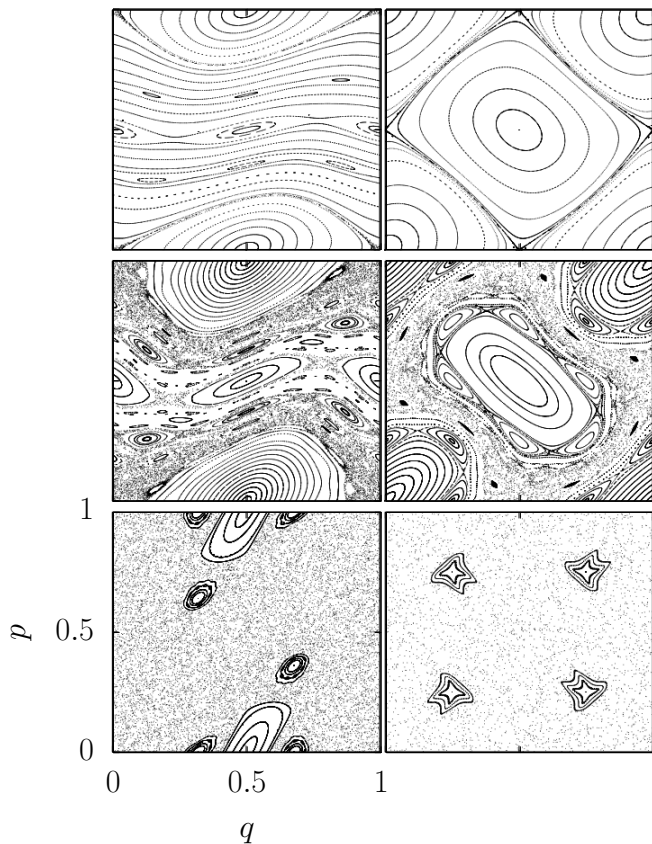


FIG. 1. Phase space portrait for the classical SM (left column) and the HM, with $K_1 = K_2 = K$ (right column) for different values of K . (top, left) $K = 0.5$, (top, right) $K = 0.1$; (center left) $K = 0.98$, (center, left) $K = 0.25$; (bottom left) $K = 2.5$, (bottom right) $K = 0.5$

for short times the decay of the average fidelity amplitude is given by

$$|\langle f(t) \rangle| \sim e^{-\Gamma t}. \quad (16)$$

For $t = 1$, in the case of the HM and the SM, Γ can be computed analytically (see appendix) and it is given by

$$\Gamma = -\ln |J_0(\delta K/\hbar)|, \quad (17)$$

where J_0 is the Bessel function. Thus when $J_0(\delta K/\hbar) = 0$, Γ diverges. It can be observed that in fact this is the case. The fidelity amplitude decays very fast for short times, and then there is a strong revival which translates in an increase of \mathcal{M}_m [17].

In Fig. 2 we show $\mathcal{M}_m(t = 200)$ for the SM (top) and the Harper map (bottom). The horizontal axis is the kicking strength K and vertical axis is the rescaled perturbation $\delta K/\hbar$. In both cases there are clearly distinguishable maxima. The horizontal dashed lines mark the points where Γ diverges, which is seen in the overlay plot of $\Gamma(\delta K/\hbar)$ (solid/gray lines). As expected along those lines \mathcal{M}_m is larger due to a large revival of the fidelity amplitude for small times.

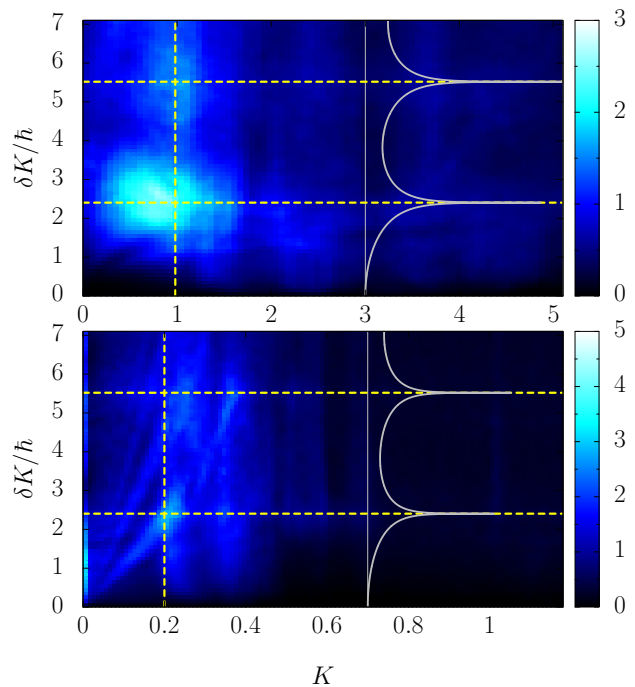


FIG. 2. $\mathcal{M}(t = 200)$ as a function of K and $\delta K/\hbar$ for the quantum standard (top) and the quantum Harper map (bottom) with $N = 500$. The vertical lines are (top) $K = 0.98 \approx K_c$, and (bottom) $K = 0.2$. Horizontal dashed lines mark the first values of δK such that $J_0(\delta K/\hbar) = 0$. Overlay (gray/solid) curves correspond to $\Gamma(\delta K/\hbar)$ from Eq. (17), rescaled to fit in the plot.

The dashed vertical line, on the other hand, marks the position of the peak on the K axis. For the SM we placed the line on the value $K_c \approx 0.98$ where the transition to unbound diffusion takes place. For the kick Harper map with $K_1 = K_2$ there is no analog transition, however we see a peak near $K = 0.2$.

In Fig 3 we show $\mathcal{M}_m(t)$ as a function of K for the case $\delta K/\hbar = 2.0$. Panels on the left (right) correspond to the SM (HM). On the top we consider the dependence with time. It is clear that for a fixed dimension N , as time increases the peak establishes at a fixed value. The good scaling with t_{\max} (after the peak) can be explained as follows: as the environment becomes more chaotic, the fidelity decays faster and fluctuates around a constant value. As a consequence, the growth of $\mathcal{M}_m(t)$ becomes linear in time – much sooner for a chaotic environment –, with a slope proportional to $(1/N)$ [17]. So for a fixed N , the curves should scale with time. The discrepancy for short t is understood because the linear regime is probably not yet attained. On the bottom row of Fig 3 we explore the possibility of finite size effects. We show $\mathcal{M}_m(t = 2000)$ with a fixed t . As N grows the peak settles at a constant value – again $K \approx 0.98$ for the SM and $K \approx 0.2$ for the HM (both marked by the limit of the shaded region).

We conclude this section by stating that $\mathcal{M}_m(t)$, which

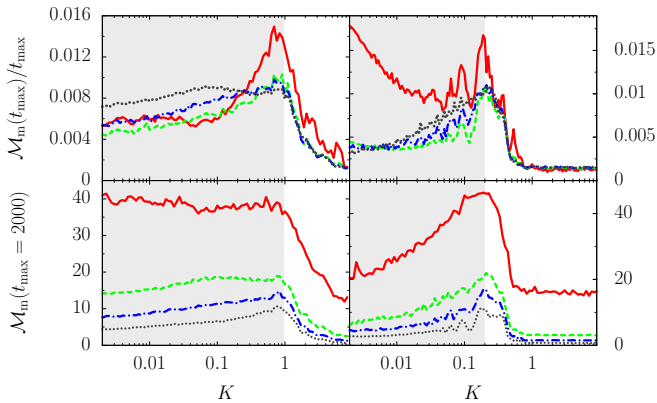


FIG. 3. Top row: $\mathcal{M}_m(t_{\max})/t_{\max}$ as a function of the kicking strength K with $N = 512$, for different times $t_{\max} = 100$ (solid/red), 500 (dash/green), 1000 (dot-dash/blue), 4000 (dot/gray) for (Left) SM. (Right) HM. Bottom row: $\mathcal{M}_m(t_{\max} = 2000)$ as a function of K , for different environment sizes $N = 100$ (solid/red), $N = 500$ (dash/green), $N = 1000$ (dot-dash/blue), and $N = 2000$ (dot/gray) for (Left) SM and (Right) HM. In all cases $\delta K/\hbar = 2.0$

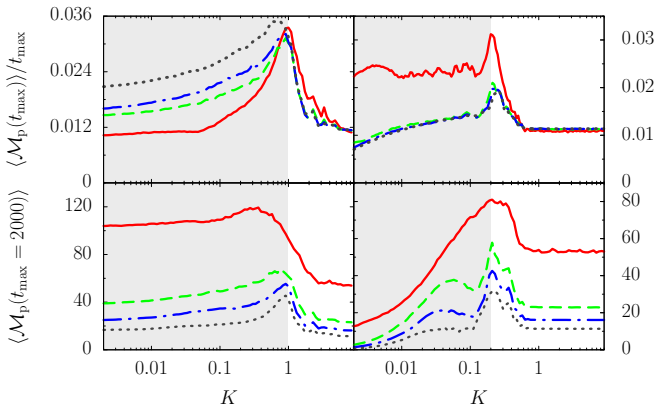


FIG. 4. Same as Fig. 3 for $\mathcal{M}_p(t)$

depends on the fluctuations of the average fidelity amplitude, seems to be reinforced at a classically significant point in parameter space for the SM, namely K_c . On the other hand for the HM we make a complementary remark. Since the peak at $K = 0.2$ seems to be robust (both changing N and t_{\max} , we conjecture that in analogy to K_c of the SM there should be a similar transition, at least in some global property of the classical map, near $K = 0.2$. We postpone that discussion until Sec. V C.

V. ENVIRONMENT IN A PURE STATE: CLASSICAL PHASE SPACE REVEALED

In the previous section we obtained unintuitive results for the non-Markovianity when the dynamics of the environment goes from integrable to chaotic. In particular there appears to be maxima of \mathcal{M}_m as a function of K

(and δK). To obtain these results, we chose the initial state of the environment to be in a maximally mixed state so the measure $\mathcal{M}_m(t)$ depends on the average fidelity amplitude (see Eq. (9)). This average is a sum of amplitudes and interference effects could be argued to be at the origin of the peaks observed. For completeness, in this section we suppose the environment to be initially in a pure state [9], in particular a Gaussian – or coherent – state, using $\mathcal{M}_p(t)$ of Eq. (8), for two reasons. First to contrast the global properties obtained with $\mathcal{M}_m(t)$, through the average behavior of the fidelity. But also, to show that $\mathcal{M}_p(t)$, and as a consequence fidelity fluctuations, as a function of the center of the initial Gaussian wave packet, gives a precise image of the classical phase portrait.

A. Correspondence between \mathcal{M}_m and $\langle \mathcal{M}_p \rangle$

In this section we contrast the results for $\mathcal{M}_m(t)$ in Sect. IV with the ones for the average of $\mathcal{M}_p(t)$. We consider a uniform grid of N points at positions $q_i = i/\sqrt{N}$, $p_j = j/\sqrt{N}$ and place coherent state centered at each pair q_i, p_j . We then average over all the initial states of the environment and get

$$\langle \mathcal{M}_p(t) \rangle = \frac{1}{N} \sum_{i=0}^{\sqrt{N}-1} \sum_{j=0}^{\sqrt{N}-1} \mathcal{M}_p^{(q_i, p_j)}(t), \quad (18)$$

where $\mathcal{M}_p^{(q_i, p_j)}(t)$ is just $\mathcal{M}_p(t)$ for a particular Gaussian state centered at (q_i, p_j) .

In Fig. 4 we show for $\langle \mathcal{M}_p(t) \rangle$ the curves for the parameters that correspond to the ones obtained in Fig. 3. As expected the curves are different, but the qualitative properties are very similar. Mainly the marked peak at $K \approx 0.98$ for the SM and at $K \approx 0.2$ for the HM are preserved. On the top row, we observe that after the peak the scaling with t_{\max} also holds. On the bottom row the dependence with N is shown. It is also clear that the peak becomes more defined as N grows.

B. Classical phase space sampling using \mathcal{M}_p

In the previous sections we have shown (Figs. 3 and 4) that qualitatively there is no difference between the non-Markovianity for the environment and in a completely mixed state and the average non-Markovianity for the environment in a pure state. This is what we called global feature, “global” referring to an average over states covering the whole phase space. The only difference is whether we do the average over amplitudes (\mathcal{M}_m) or probabilities (\mathcal{M}_p). Nevertheless for individual pure states of the environment, non-Markovianity is strongly state-dependent. In this section we seek to show this dependence is strongly related to the details of the classical phase space portrait of the environment. For this, we again define a grid of n_s points

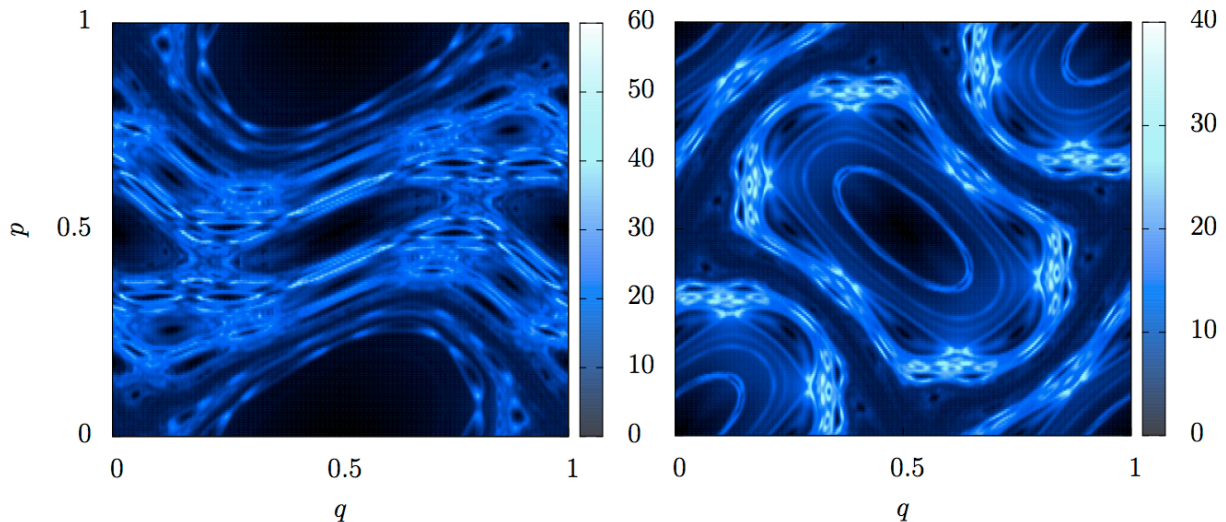


FIG. 5. $\mathcal{M}_p(t)$ as a function of the center (q_0, p_0) of the initial Gaussian wave packet with $N = 5000$, $\delta K/\hbar = 2$ and $t = 500$ for the SM with $K = 0.98$ (left) and the HM with $K = 0.25$ (right).

$q_i, p_j = 0, 1/\sqrt{n_s}, \dots, (\sqrt{n_s} - 1)/\sqrt{n_s}$. We then compute $\mathcal{M}_p(t)$ for a fixed time, and we plot this as a function of initial position and momentum. In other words we plot $\mathcal{M}_p^{(q_i, p_j)}(t)$ from Eq. (18). The results obtained were surprising. We did expect that the classical dynamics should have some kind of effect. However we did not expect that \mathcal{M}_p would reproduce with such detail the complexities of the classical phase space. In Fig. 5 it is shown how all the classical structures are very well reproduced by the landscape built from $\mathcal{M}_p(t)$ as a function of q_i and p_j (see the corresponding classical cases in Fig. 1). Of course, the ability to resolve classical structure will be limited by two factors: the dimension N (or equivalently, size of effective \hbar), and the number of initial states n_s (or “pixels”). In Fig. 5 it could be argued that $N = 5000$ is almost classical. This argument becomes relative when one considers that a quantum map with $N \approx 5000$ could be implemented in a quantum computer of the order of, a little more than, 12 qubits (not a very big number of particles).

But the most surprising thing is that, contrary to intuition, $\mathcal{M}_p(t)$ is almost as small for a regular environment (i.e. when the initial state is localized inside a regular island) as for chaotic a chaotic environment. On the contrary $\mathcal{M}_p(t)$ exhibits peaks at the regions that separate different types of dynamics. Specifically at the complex areas consisting of broken tori that separate regular islands and chaotic regions and near hyperbolic periodic points. This means that the main contribution to the average non-Markovianity (in the mixed phase space case) does not come from the regular parts. In Fig. 6 we show a two dimensional curve that corresponds to a detail of the HM case in Fig. 5. Two things can be directly observed. The first one is how \mathcal{M}_p becomes larger and has maxima in the regions that lie between regular and chaotic behavior. But also how larger N resolve

better the small structures. In particular elliptic periodic points are expected to be a minimum of \mathcal{M}_p because they are structurally stable and so a small perturbation leaves them unchanged. In that case fidelity does not decay, or decays very slowly. The dashed (blue) line ($N = 1000$) detects the change between regular and chaotic, but does not resolve the structure inside the island. In this case the width of a coherent state ($1/\sqrt{N}$) is of the order, or larger, than the size of the island. On the contrary, for larger N (red line) the structure inside the island is well resolved and \mathcal{M}_p has maxima on the borders of the island and is minimal on top of the periodic point.

So from the numerical results we conclude that the main contribution to non-Markovian behavior comes from the regions of phase space that delimit two separate regions – like chaotic and regular regions, and also two disjoint regular islands. The relation with the fidelity is key to understanding this effect. For states in the chaotic region the fidelity decays exponentially and saturates at a value which depends on the size of the chaotic area (typically proportional of order $1/N$). The main contribution to non-Markovianity for chaotic initial conditions come from small time revivals (see e.g. [49]). The contribution due to fluctuations around the saturation value grows linearly with time, but with a slope that is inversely proportional to N , so in the large N limit it can be neglected. Gaussian initial states inside regular islands evolve in time with very small deformation, so the fidelity is expected to decay very slowly and eventually there will be very large (close to 1) revivals. However the large revivals will be sparse and their contribution to non-Markovianity will be small. In the border areas there is no exponential spreading so the initial decay is slower, and there is no chaotic region so there is no expected saturation. As a result after a short time decay we observe numerically that there are high frequency fluctu-

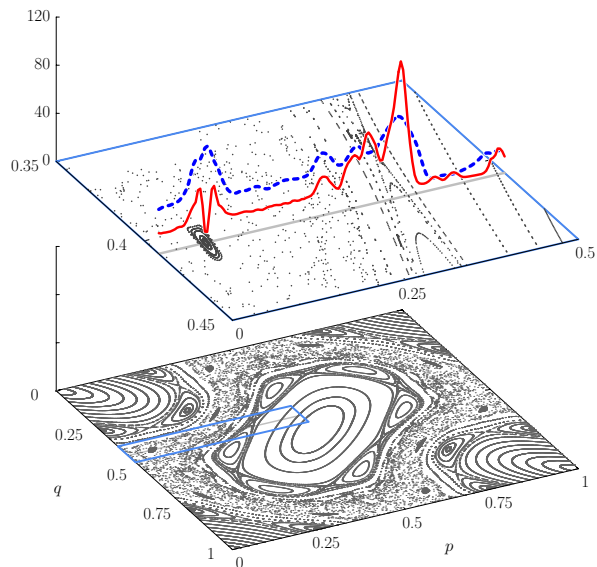


FIG. 6. $\mathcal{M}_p(t = 2000)$ as a function of initial position ($q_0 = 0.408171$, $p_0 \in [0, 0.5]$) of the state of the environment and two different dimensions (red/solid) $N = 4000$, (blue/dashed) $N = 1000$. The map is the quantum HM with $K = 0.25$, $\delta K/\hbar = 2$. The blue square on the bottom indicates the area that is detailed above.

ations that contribute strongly to the non-Markovianity measure.

We illustrate this in Figs. 7 and 8. In Fig. 7 we show $\mathcal{M}_p(t = 1000)$ for the HM with coherent states centered at $q = p$. There is a minimum at the fixed point which is understood again in terms of structural stability: when the map is perturbed, the fixed point remains a fixed point, so fidelity does not decay. To further understand we use Fig. 8 where we show the fidelity and $\mathcal{M}_p(t)$ for the two points marked in Fig. 7 (circle: $q_0 = p_0 = 0.05$; square: $q_0 = p_0 = 0.275$). Inside the islands the motion of the wave packets is more or less classical with little stretching over long times. Fidelity decays slowly and since there is practically no deformation, there are large revivals at times of the order of N (solid/red curve in Fig. 8 top). On the contrary at the separatrix the wave packets spread and though initially fidelity decays fast, there remains a significant overlap the whole time. The complex motion accounts for the fluctuations (dashed/blue curve in Fig. 8 top) and the resulting maximum of \mathcal{M}_p seen in Fig. 7.

C. Compatibility with classical results

The results obtained in the previous sections relate NM with some global property of the classical system. For the standard map there is a critical value K_c of the kicking strength after which the motion in the momentum direction (when the map is taken in the cylinder) becomes unbounded. This value, estimated to be $K_c = 0.971635\dots$

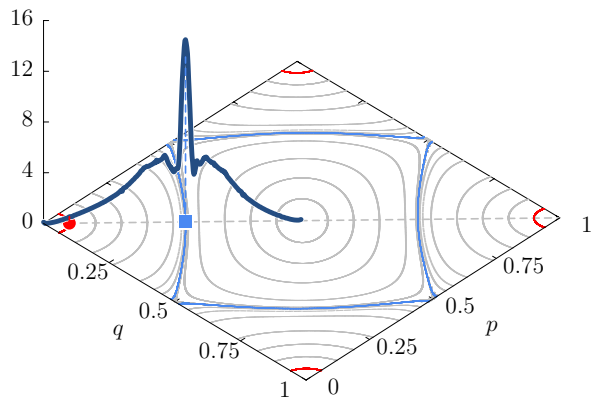


FIG. 7. $\mathcal{M}_p(t = 1000)$ as a function of the position $q_0 = p_0$ of the initial state of the environment. The map is the quantum HM with $N = 2000$, $K = 0.1$, $\delta K/\hbar = 2$. Dark lines are the classical trajectories corresponding to the to curves shown in Fig. 8.

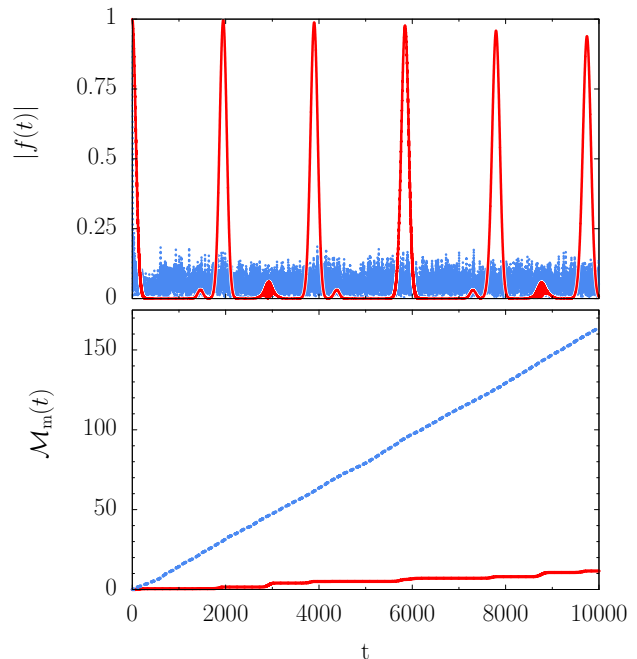


FIG. 8. Top: $|f(t)|$ for two coherent states evolved with the quantum HM for $K = 0.2$, $\delta K/\hbar = 2.0$ and $N = 2000$. (blue) $q_0 = p_0 = 0.275$ corresponds to the maximum seen in Fig. 7, and (red) $q_0 = p_0 = 0.05$.

[45], corresponds to the breaking of the torus with most irrational winding number.

Motion for the kicked Harper map on the contrary is different. For $K = 0$ it is integrable with a separatrix joining the unstable fixed points $(0, 1/2)$, $(1/2, 0)$, $(1, 1/2)$, $(1/2, 1)$. For $K > 0$ the separatrix breaks and – if considered on the whole plane – a mesh of finite width forms, also called stochastic web. Motion inside this mesh is chaotic and diffusion is unbounded for all K .

Although –to our knowledge – for the HM there is no critical K analog to K_c for the standard map, the peaks in Figs. 2, 3, and 4 hint that there could exist a similar kind of transition function of K . To test this conjecture we evaluate two different global quantities. First we take into account diffusion. Considering the map on the whole plane (i.e. no periodic boundaries) if diffusion is normal then the spreading, e.g. in momentum, should grow linearly with time (number of kicks). Thus we define

$$D = \lim_{t \rightarrow \infty} \frac{\langle (p_t - p_0)^2 \rangle}{t}, \quad (19)$$

where the average is taken over each initial condition. In the $t \rightarrow \infty$ limit, $D \rightarrow 0$ if diffusion is bounded. So, for the SM we expect D to be 0 (or go to 0 with time) below K_c and start growing for $K > K_c$. For the HM we do not know a theoretical value of K_c .

However, the diffusion coefficient D depends only on the unperturbed motion. We therefore propose a measure that depends the distance between perturbed and unperturbed trajectories and that is built to resemble \mathcal{M} . We take an initial point (q_0, p_0) and evolve it with the classical map, without periodic boundary conditions, and we measure the distance

$$d_t = \sqrt{(q_t - q'_t)^2 + (p_t - p'_t)^2} \quad (20)$$

as a function of (discrete) time t , with q' , p' the perturbed trajectories. Finally in order to mimic the behavior of quantum fidelity we take

$$\tilde{f}_t = \exp[-d_t] \quad (21)$$

which is equal to 1 for $t = 0$ and decays for $t > 0$. For chaotic motion, e.g. on the stochastic web defined by the HM $\tilde{f}_t \rightarrow 0$ as $t \rightarrow \infty$. In analogy with (8) and (9), we define

$$\tilde{\mathcal{M}}(t) = \sum_{f_t - f_{t-1} > 0} (f_t - f_{t-1}). \quad (22)$$

The value of this quantity becomes apparent in the light of numerical results. In Fig. 9 we show \mathcal{M}_m , \mathcal{M}_p (top row) and $\tilde{\mathcal{M}}$ (middle row) as a function of K for both the SM and the HM. In the middle row we see $\tilde{\mathcal{M}}$ for both maps for two different times. There is a qualitatively similar behavior to \mathcal{M}_p (on the top row) where $\tilde{\mathcal{M}}$ grows with K until it reaches a peak at K^* , and then after that it decreases. We have already hinted that for the SM, this peak is reached for $K^* \approx K_c$, where the last irrational torus is broken, or when unbounded diffusion sets in. We know that $K_c \approx 0.98$ [44, 45]. For the symmetric HM there is both normal and anomalous diffusion, described in [50], but there is *a priori* no equivalent point to K_c of the SM.

On the bottom row of Fig. 9 we show the numerical calculation of the diffusion coefficient D , defined in Eq. (19), by evolving a number of initial conditions up to a time t and compute the slope of $\langle (p_t - p_0)^2 \rangle / t$. The red/solid

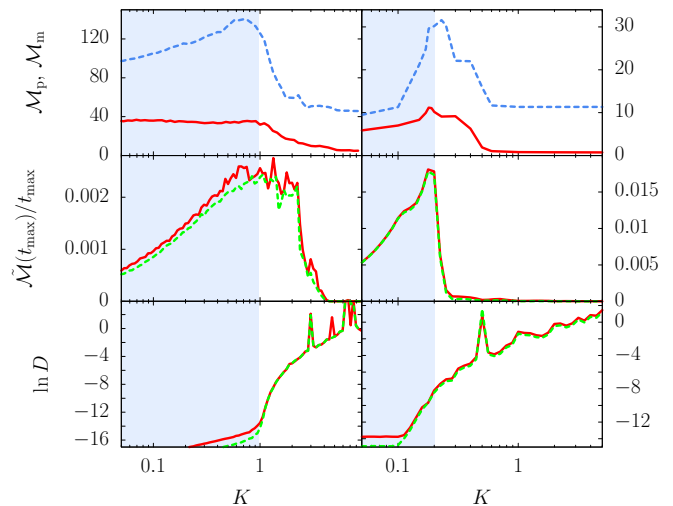


FIG. 9. Top Row: \mathcal{M}_p (dashed/blue) and \mathcal{M}_m (solid/red) as a function of K for the SM (left) and the HM (right) with $N = 512$, $\delta K/\hbar = 2.0$, and $t_{\max} = 4000$. Middle Row: $\tilde{\mathcal{M}}/t_{\max}$ as a function of K for the SM (left) and the HM (right) with $t_{\max} = 20000$ (red/solid) and 50000 (green/dashed). Bottom Row: D as a function of K for the SM (left) and the HM (right) with $t_{\max} = 20000$ (red/solid) and 50000 (green/dashed). The limit of the shaded area is $k = 0.98$ (SM) and $K = 0.2$ HM.

line corresponds to $t = 1000$ while the green/dashed line corresponds to $t = 16000$. It is clear that after the critical point (marked by the shaded region) both curves for D are approximately the same, while $D \rightarrow 0$ for $K < 0.98$, as expected. For the HM the situation is similar but the critical point obtained numerically ($K \approx 0.1$) differs from $K^* \approx 0.2$. Thus, for the HM, there is no apparent relation between the maxima observed in the first and second rows of Fig. 9 and diffusion. We should however note that diffusion in the Harper (with $K_1 = K_2$) and standard maps is fundamentally different.

VI. CONCLUSION

We studied numerically the non-Markovian behavior of an environment modeled by a quantum kicked map, when it interacts – pure dephasing – with a system consisting of a qubit. In particular we centered our attention on the transition from regular to chaotic dynamics. At the extremes, i.e. either regular or chaotic the behavior is as expected: if the environment is chaotic then we expect it to lose memory quicker and be more Markovian than an environment corresponding to regular dynamics. At the transition, where classical dynamics is mixed, unexpected behavior manifests in the form of a peak. In the case of the standard map the peak is located almost exactly at the critical point where the last irrational torus breaks and for dynamics in the cylinder there is unbounded diffusion. For the case of the Harper map, there is no crit-

ical point. However we obtain a peak that is robust to changes in size, time and way of averaging. We conjecture that it should also correspond to a transition point in the classical dynamics. To support this conjecture we studied the fluctuations of the distance between classical trajectories (with no periodic boundaries). We found peaks at locations compatible with the results obtained for the non-Markovianity measure used.

Additionally, by studying the dependence of non-Markovianity on the initial state of the environment we first found that the main contributions to average non-Markovian behavior come, not from regular (integrable) islands, but from the regions between chaotic and integrable which typically are complex and composed of broken tori. We were able to build classical phase space pictures from the non-Markovianity measure, where the borders between chaos and regularity are clearly highlighted. It is worth remarking that from our numerical investigations yet another feature of quantum fidelity has been unveiled: the long time fluctuations can help identify complex phase space structures like the border between chaotic and regular regions. Traditional (average) fidelity decay approaches have the aim of identifying sensitivity to perturbations, and chaos. The approach presented here, in contrast, can – from the fidelity as a function of each individual initial state – provide a clear image of the classical phase portrait and not just a global quantity from which to infer chaotic (or regular) behavior.

Finally, we think that our numerics fit well within the scope of recent experimental setups [22], and some of our findings could be explored.

ACKNOWLEDGMENTS

C.P. received support from the projects CONACyT 153190 and UNAM-PAPIIT IA101713. I.G.M. and D.A.W. received support from ANCyPT (PICT 2010-1556), UBACyT, and CONICET (PIP 114-20110100048 and PIP 11220080100728).

Appendix A: Semiclassical expression for short time decay of the fidelity amplitude

The fidelity or Loschmidt echo is the quantity originally proposed by Peres [51] to characterize sensitivity of a system to perturbation and then used to characterize quantum chaos. It is defined as

$$M(t) = |f(t)|^2 \quad (\text{A1})$$

where

$$f(t) = \langle \psi_0 | e^{iH_\epsilon t/\hbar} e^{-iH_0 t/\hbar} | \psi_0 \rangle \quad (\text{A2})$$

where H_ϵ differs from H_0 by a perturbation term, usually taken as an additive ϵV term, with ϵ a small number.

Using the initial value representation for the Van Vleck semiclassical propagator and a concept known as dephasing representation (DR), justified by the shadowing theorem, recently the following simplified semiclassical expression for the fidelity amplitude to [52–54] was obtained

$$f_{\text{DR}}(t) = \int dqdp W_\psi(q, p) \exp(-i\Delta S_\epsilon(q, p, t)/\hbar). \quad (\text{A3})$$

In Eq. (A3) $W_\psi(q, p)$ is the Wigner function of the initial state ψ and

$$\Delta S_\epsilon(q, p, t) = -\epsilon \int_0^t d\tau V(q(\tau), p(\tau)) \quad (\text{A4})$$

is the action difference evaluated along the *unperturbed* classical trajectory.

For sufficiently chaotic system we can approximate the dynamics as random-uncorrelated and express the average fidelity amplitude as [49]

$$\langle f_{\text{DR}}(t) \rangle = \left[\frac{1}{N} \sum_j \exp(-i\Delta S_{\epsilon, j}/\hbar) \right] \quad (\text{A5})$$

the average is done over a complete set labeled j (N is the dimension of the Hilbert space) and $\Delta S_{\epsilon, j}$ is the action difference for the state j at time $t = 1$ (we focus on discrete time (maps), so for us it means after one step). For large enough N we can approximate by a continuous expression

$$\langle f_{\text{DR}}(t) \rangle \approx \left(\int dqdp \exp[-i\Delta S_\epsilon(q, p)/\hbar] \right)^t \quad (\text{A6})$$

The short time decay of the AFA can be approximated by

$$|\langle f(t) \rangle| \approx e^{-\Gamma t} \quad (\text{A7})$$

with

$$\Gamma \approx -\ln \left| \int dqdp \exp[-i\Delta S_\epsilon(q, p)/\hbar] \right| \quad (\text{A8})$$

This expression is exact for $t = 1$ and is valid for larger times the more chaotic is the system (see [49]). For both maps in Eqs. (12) and (14) we have $V = K \cos[2\pi q]$ so

$$\Gamma \approx -\ln \left| \int dq e^{-(\delta K/\hbar) \cos[2\pi q]} \right| = -\ln [|J_0(\delta K/\hbar)|], \quad (\text{A9})$$

where J_0 is the Bessel function of the first kind (with $n = 0$), which is an oscillating function. When $J_0 = 0$, Γ diverges. This means that near these values for short times fidelity decays almost to zero. Nevertheless – also depending on how chaotic is the system – after this strong decay, typically there is a large revival [49, 55].

-
- [1] W. H. Zurek, *Rev. Mod. Phys.* **75**, 715 (2003).
- [2] G. Lindblad, *Comm. Math. Phys.* **48**, 119 (1976).
- [3] V. Gorini, A. Kossakowski, and E. C. G. Sudarshan, *J. Math. Phys.* **17**, 821 (1976).
- [4] H.-P. Breuer and F. Petruccione, *The Theory of Open Quantum Systems* (Oxford University Press, Oxford, 2007).
- [5] S. Daffer, K. Wódkiewicz, J. D. Cresser, and J. K. McIver, *Phys. Rev. A* **70**, 010304 (2004).
- [6] H.-P. Breuer, E.-M. Laine, and J. Piilo, *Phys. Rev. Lett.* **103**, 210401 (2009).
- [7] A. Rivas, S. F. Huelga, and M. B. Plenio, *Phys. Rev. Lett.* **105**, 050403 (2010).
- [8] M. Žnidarič, C. Pineda, and I. García-Mata, *Phys. Rev. Lett.* **107**, 080404 (2011).
- [9] P. Haikka, J. Goold, S. McEndoo, F. Plastina, and S. Maniscalco, *Phys. Rev. A* **85**, 060101 (R) (2012).
- [10] G. Clos and H.-P. Breuer, *Phys. Rev. A* **86**, 012115 (2012).
- [11] S. Alipour, A. Mani, and A. Reza khani, *Phys. Rev. A* **85**, 052108 (2012).
- [12] P. Zhang, B. You, and L.-X. Cen, arxiv:1302.6366.
- [13] B. Bylicka, D. Chruściński, and S. Maniscalco, arxiv:1301.2585.
- [14] B.-H. Liu, L. Li, Y.-F. Huang, C.-F. Li, G.-C. Guo, E.-M. Laine, H.-P. Breuer, and J. Piilo, *Nat. Phys.* **7**, 931 (2011).
- [15] A. Chiuri, C. Greganti, L. Mazzola, M. Paternostro, and P. Mataloni, *Scientific Reports* **2**, 968 (2012).
- [16] B.-H. Liu, D.-Y. Cao, Y.-F. Huang, C.-F. Li, G.-C. Guo, E.-M. Laine, H.-P. Breuer, and J. Piilo, *Scientific Reports* **3**, 1781 (2013).
- [17] I. García-Mata, C. Pineda, and D. A. Wisniacki, *Phys. Rev. A* **86**, 022114 (2012).
- [18] A. de Almeida, *Hamiltonian Systems: Chaos and Quantization*, Cambridge Monographs on Mathematical Physics (Cambridge University Press, 1990).
- [19] Z. P. Karkuszewski, C. Jarzynski, and W. H. Zurek, *Phys. Rev. Lett.* **89**, 170405 (2002).
- [20] H. Quan, Z. Song, X. Liu, P. Zanardi, and C. Sun, *Phys. Rev. Lett.* **96**, 140604 (2006).
- [21] G. B. Lemos and F. Toscano, *Physical Review E* **84**, 016220 (2011).
- [22] G. B. Lemos, R. M. Gomes, S. P. Walborn, P. H. S. Ribeiro, and F. Toscano, *Nature Communications* **3**, 1211 (2012).
- [23] D. Poulin, R. Blume-Kohout, R. Laflamme, and H. Ollivier, *Phys. Rev. Lett.* **92**, 177906 (2004).
- [24] T. Gorin, T. Prosen, T. Seligman, and M. Žnidarič, *Phys. Rep.* **435**, 33 (2006).
- [25] Ph. Jacquod and C. Petitjean, *Adv. Phys.* **58**, 67 (2009).
- [26] A. Goussev, R. Jalabert, H. M. Pastawski, and D. A. Wisniacki, *Scholarpedia* **7**, 11687 (2012).
- [27] B. Köber, U. Kuhl, H.-J. Stöckmann, T. Gorin, D. V. Savin, and T. H. Seligman, *Phys. Rev. E* **82**, 036207 (2010).
- [28] Y. Weinstein, S. Lloyd, and C. Tsallis, *Phys. Rev. Lett.* **89**, 214101 (2002).
- [29] X.-M. Lu, X. Wang, and C. P. Sun, *Phys. Rev. A* **82**, 042103 (2010).
- [30] M. M. Wolf, J. Eisert, T. S. Cubitt, and J. I. Cirac, *Phys. Rev. Lett.* **101**, 150402 (2008).
- [31] H.-S. Zeng, N. Tang, Y.-P. Zheng, and G.-Y. Wang, *Phys. Rev. A* **84**, 032118 (2011).
- [32] In our case, it is easy to see that the RHP measure, which relies on monotonous decay of entanglement in Markovian processes, differs from the BLP measure by a constant factor.
- [33] L. M. K. Vandersypen and I. L. Chuang, *Rev. Mod. Phys.* **76**, 1037 (2005).
- [34] J. Britton, B. Sawyer, A. Keith, C.-C. Wang, J. Freericks, H. Uys, M. Biercuk, and J. Bollinger, *Nature* **484**, 489 (2012).
- [35] R. A. Jalabert and H. M. Pastawski, *Phys. Rev. Lett.* **86**, 2490 (2001).
- [36] S. Wißmann, A. Karlsson, E.-M. Laine, J. Piilo, and H.-P. Breuer, *Phys. Rev. A* **86**, 062108 (2012).
- [37] S. A. Gardiner, J. I. Cirac, and P. Zoller, *Phys. Rev. Lett.* **79**, 4790 (1997).
- [38] R. Schack, *Phys. Rev. A* **57**, 1634 (1998).
- [39] B. Georgeot and D. L. Shepelyansky, *Phys. Rev. Lett.* **86**, 5393 (2001).
- [40] Y. Weinstein, S. Lloyd, J. Emerson, and D. Cory, *Physical Review Letters* **89** (2002).
- [41] B. Lévi, B. Georgeot, and D. L. Shepelyansky, *Physical Review E* **67** (2003).
- [42] B. Lévi and B. Georgeot, *Phys. Rev. E* **70**, 056218 (2004).
- [43] S. Chaudhury, A. Smith, B. E. Anderson, S. Ghose, and P. S. Jessen, *Nature* **461**, 768 (2009).
- [44] B. Chirikov and D. L. Shepelyansky, *Scholarpedia* **3**, 3350 (2008).
- [45] J. M. Greene, *J. Math. Phys.* **20**, 1183 (1979).
- [46] I. Dana, *Phys. Lett. A* **197**, 413 (1995).
- [47] R. Artuso, *Scholarpedia* **6**, 10462 (2011).
- [48] P. Leboeuf, J. Kurchan, M. Feingold, and D. Arovas, *Physical Review Letters* **65**, 3076 (1990).
- [49] I. García-Mata, R. O. Vallejos, and D. A. Wisniacki, *New J. Phys.* **13**, 103040 (2011).
- [50] P. Leboeuf, *Physica D: Nonlinear Phenomena* **116**, 8 (1998).
- [51] A. Peres, *Phys. Rev. A* **30**, 1610 (1984).
- [52] J. Vaníček and E. J. Heller, *Phys. Rev. E* **68**, 056208 (2003).
- [53] J. Vaníček, *Phys. Rev. E* **70**, 055201 (2004).
- [54] J. Vaníček, *Phys. Rev. E* **73**, 046204 (2006).
- [55] I. García-Mata and D. A. Wisniacki, *J. Phys. A: Math. Theor.* **44**, 315101 (2011).